Chemical Engineering Journal 235 (2014) 158–166

Contents lists available at ScienceDirect

Chemical Engineering Journal

journal homepage: www.elsevier.com/locate/cej

Steam-methane reforming at low temperature on nickel-based catalysts

María A. Nieva, María M. Villaverde, Antonio Monzón, Teresita F. Garetto, Alberto J. Marchi *

Catalysis Science and Engineering Research Group (GICIC), Instituto de Investigaciones en Catálisis y Petroquímica (INCAPE), FIQ-UNL-CONICET, Santiago del Estero 2654 (3000) Santa Fe, Argentina

HIGHLIGHTS

- A Ni–Zn–Al catalyst is active and stable for steam-methane reforming at low temperatures.
- Ni–Zn–Al catalyst is resistant to sintering and inhibits formation of carbonaceous deposits.
- Ni–Mg–Al catalyst is active for steam-methane reforming but produces carbon nanofibers.
- Intimate contact between Ni and spinel-like matrix is crucial for metal phase activity and stability.

GRAPHICAL ABSTRACT

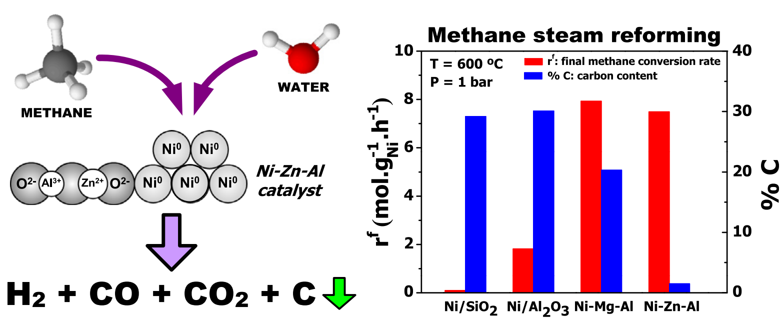

ARTICLE INFO

Article history:
Received 14 June 2013
Received in revised form 22 August 2013
Accepted 4 September 2013
Available online 12 September 2013

Keywords:
Steam-methane reforming
Nickel catalysts
Metal–support interaction
Synthesis gas
Hydrogen

ABSTRACT

In this work, we report the activity results obtained in steam-methane reforming (SMR) at 500 and 600 °C using four nickel-based catalysts: (a) Ni/α-Al_2O_3 and Ni/SiO_2, prepared by incipient wetness impregnation method and (b) Ni–Zn–Al and Ni–Mg–Al, prepared by coprecipitation method. In all of the samples, the nickel load ranged between 7% and 9%. The catalytic activity in SMR at steady state followed the pattern: Ni–Mg–Al $\cong$ Ni–Zn–Al > Ni/α-Al_2O_3 > Ni/SiO_2. According to characterization results, the interaction between Ni^{2+} species and support in precursor oxides was stronger in Ni–Mg–Al and Ni–Zn–Al than in Ni/α-Al_2O_3 and Ni/SiO_2. After activation in H_2 flow, large metal nickel particles with low or none interaction with the support were obtained in the case of Ni/α-Al_2O_3 and Ni/SiO_2. On the contrary, small metal particles, between 3 and 6 nm, in high interaction with support were obtained in Ni–Zn–Al and Ni–Mg–Al catalysts. The metal phase formed in Ni–Mg–Al and Ni–Zn–Al was the most active and resistant to sintering under reaction conditions at $T \leqslant 600$ °C. It was also found that carbon nanofibers were formed on Ni/α-Al_2O_3, Ni/SiO_2 and Ni–Mg–Al catalysts during SMR at 600 °C. The amount and diameter of nanofibers formed on Ni–Mg–Al were lower than on catalysts prepared by impregnation method, which is in agreement with the relative sizes of metal nickel particles in each case. Amazingly, no filamentary carbon was detected on the used Ni–Zn–Al sample: only amorphous coke in low amounts was formed. This was attributed to the proper interaction of small metal nickel particles with the non-stoichiometric zinc aluminate-like phase formed after thermal treatments of catalyst precursor.

1. Introduction

Steam-methane reforming (SMR) is the most common process at industrial scale for the production of hydrogen and synthesis gas [1]. In particular, according to the US DOE, almost 95% of the hydrogen is produced in United States by SMR [2]. This process is employed in both petrochemical industry and energy production. For example, synthesis gas produced via steam reforming is employed in order to obtain the reducing gas for steel production and also as raw material in the ammonia, methanol and Fischer–Tropsh synthesis [1–4].

* Corresponding author. Tel.: +54 342 4533858; fax: +54 342 4531068.
E-mail address: amarchi@fiq.unl.edu.ar (A.J. Marchi).

1385-8947/$ - see front matter © 2013 Elsevier B.V. All rights reserved.
http://dx.doi.org/10.1016/j.cej.2013.09.030

The principal products in SMR are CO, CO_2 and H_2, which are produced according to reactions (1) and (2), being the first reaction highly endothermic and the second one slightly exothermic.

$$CH_4 + H_2O \Longleftrightarrow CO + 3H_2 \quad \Delta H^0(25\,^\circ C) = 2062\ kJ\ mol^{-1} \tag{1}$$

$$CO + H_2O \Longleftrightarrow CO_2 + H_2 \quad \Delta H^0(25\,^\circ C) = -412\ kJ\ mol^{-1} \tag{2}$$

Simultaneously, CO disproportionation (3) and CH_4 decomposition (4) can take place, which are undesirable reactions because they produce carbon deposits and whiskers [5]. Both reactions can take place between 500 and 600 °C, but CO disproportionation is thermodynamically favored against CH_4 decomposition in this temperature range [3].

$$2CO \Longleftrightarrow C(s) + CO_2 \quad \Delta H^0(25\,^\circ C) = -1724\ kJ\ mol^{-1} \tag{3}$$

$$CH_4 \Longleftrightarrow C(s) + 2H_2 \quad \Delta H^0(25\,^\circ C) = 749\ kJ\ mol^{-1} \tag{4}$$

Since reaction (1) is highly endothermic, it is necessary to carry out the SMR process at high temperatures in order to reach complete methane conversion. Normally, the temperature at the reformer inlet is between 450 and 600 °C while at the outlet it is in the range of 850–950 °C [4]. Water–gas shift (WGS) reaction and CO disproportionation, Eqs. (2) and (3), respectively, are thermodynamically favored in the reformer low temperature region while CH_4 decomposition, equation (4), is favored in the high temperature zone.

There are many research papers in which the use of different type of metal-based catalysts and reactors were proposed with the aim of improving H_2 production and to minimize coke formation in methane reforming [4–29]. The most used catalysts were those based on noble and non-noble metals of group VIII. Among them, nickel is the preferred one in industrial applications due to its low cost and catalytic performance [4,6]. However, the C(s) produced by reactions (3) and (4) can be dissolved in the metal nickel particles and diffuse through it to form carbon whiskers [4]. If these whiskers are produced in large amounts, they can break-up the catalyst pellets and produce large amounts of powder. This will increase the pressure drop in the catalyst bed leading to operational problems in the reformer unit [7]. Formation of carbonaceous deposits is favored below a critical steam to carbon (S/C) ratio [4,6]. Therefore, S/C ratios used at industrial scale are higher than unity. Normally, values between 2.5 and 4.5 are used at the inlet of industrial reformers in order to reduce carbon production [2]. An alternative to control carbon deposit formation is the use of a pre-reformer unit that normally works between 400 and 600 °C [2,3]. The idea is to carry out the methane conversion under conditions that insure the inhibition of reactions (3) and/or (4). One proposal to fulfill this objective is to use a catalyst formed by a stable phase of metal nanoparticles being active at 500–600 °C for reaction (1) but that inhibits reactions (3) and (4).

The support and metal–support interaction are also influencing the formation of carbonaceous deposits and carbon whiskers during SMR process. The most common supports used in the open literature for SMR are α-Al_2O_3, γ-Al_2O_3, SiO_2, MgO, $MgAl_2O_4$, CeO_2, TiO_2 and ZrO_2 [8–18]. In some cases, surface acid sites are present and they promote hydrocarbon cracking and subsequent polymerization leading to formation of carbonaceous deposits on the catalyst surface [19]. Then, a way to suppress carbon deposition on Ni-based catalysts is by adding an alkali metal. However, addition of alkali promoters can decrease catalyst activity [20]. Then, it would be better to design the catalyst having the right acid–basic properties and the proper metal–support interaction in order to inhibit the formation of carbonaceous deposits.

Another aspect that must be taken into account for the design of a SMR catalyst is the particle sintering, since this is also one possible cause for catalyst deactivation. It is well known that the rate and extent of sintering depend on many factors, as for example metal load, crystallite size, support nature and reaction conditions. The most accepted mechanism for particle sintering is migration and coalescence [21]. In order to avoid particle migration on support surface, the interaction between metal nanoparticles and support must be the proper one. In this sense, a stable metal phase highly dispersed in a Ni–Mg–Al oxide was obtained from a hydrotalcite-like precursor [17,22]. In other cases, a noble metal phase highly dispersed in a Mg–Al oxide matrix was obtained following similar procedures [23,24].

In summary, the challenge is to design and develop a catalyst active in SMR at low temperature, resistant to sintering and with low formation of carbon deposits. In a previous paper, we studied the hydrogenation of acetylene with Ni-based catalyst having a non stoichiometric spinel-like structure and the carbon formation was considerably reduced respect to other Ni-based catalysts [30]. In this work we study the SMR at 500–600 °C over Ni–Mg–Al and Ni–Zn–Al catalysts, prepared by coprecipitation method, and compared their catalytic performance with that of Ni supported on SiO_2 and α-Al_2O_3, prepared by incipient wetness impregnation. The objective in this work is to obtain a stable phase of metal nickel nanoparticles with high activity for SMR, able to inhibit carbon production at temperatures below 600 °C and simultaneously resistant to sintering under reaction conditions. This catalyst could be useful in the low temperature range of a steam reformer or in a pre-reformer unit.

2. Experimental

2.1. Catalyst preparation

Two catalysts, Ni/SiO_2 (NS) and Ni/α-Al_2O_3 (NA), were prepared by incipient wetness impregnation using as supports SiO_2 (Aldrich, $Sg = 250\ m^2\ g^{-1}$) and α-Al_2O_3 (Aldrich, $Sg = 8\ m^2\ g^{-1}$). A 0.5 M solution of $Ni(NO_3)_2 \cdot 6H_2O$ (Merck, for analysis) was added dropwise to the supports, previously calcined in air during 4 h at 500 °C. These hydrated precursors were dried in an oven at 100 °C for 12 h and then calcined in air flow (60 $cm^3\ min^{-1}$) at 400 °C for 6 h. Other two Ni-based catalysts, Ni–Mg–Al (NMA) and Ni–Zn–Al (NZA), were prepared by the co-precipitation technique according to the procedure described elsewhere [30,31]. The atomic ratios in samples NMA and NZA were $Zn(Mg)/Ni \cong 3$ and $Zn(Mg)/Al \cong 0.75$. An aqueous solution containing a mixture of the corresponding nitrates and a basic aqueous solution of K_2CO_3 (for NZA) or $K_2CO_3/KOH = 0.125$ (for NMA) were simultaneously added dropwise to 400 ml of distilled water at 60 °C while the pH was kept at 7.2 ± 0.2 for NZA and 10 ± 0.2 for NMA. The resulting precipitates were aged for 1 h at 60 °C in the mother liquor and then filtered, washed with deionized water at 60 °C and dried at 80 °C overnight. The hydrated precursors were decomposed in N_2 flow (60 $cm^3\ min^{-1}$) at 500 °C for 5 h to obtain the corresponding mixed oxides.

2.2. Catalyst characterization

Specific surface area (Sg) were measured by N_2 physisorption at −196 °C in a Quantachrome Autosorb I sorptometer. Elemental composition of the samples was determined by atomic absorption spectrometry (AA) using a Perkin Elmer Spectrometer AAnalyst 800. Hydrogen chemisorption was measured via volumetric adsorption experiments at room temperature in a conventional vacuum apparatus using the method described elsewhere [31,32].

The reducibility of the calcined samples were determined by temperature-programmed reduction (TPR) using a Micromeritics Auto Chem II 2920 V2.00. The TPR profiles were acquired passing a H_2 (5%)/Ar flow (60 $cm^3 min^{-1}$) while the samples were heated from room temperature to 950 °C at 10 °C min^{-1}.

Surface acidity was determined by temperature-programmed desorption of NH_3 (NH_3-TPD). Samples (100 mg) were pretreated by heating in He (60 $cm^3 min^{-1}$) flow from 25 °C to 300 °C at 10 °C min^{-1} and keeping the final temperature for 1 h. Then, samples were cooled down to 100 °C and exposed to an NH_3(1%)/He gaseous stream for 1 h. The physisorbed NH_3 was removed by flowing He (60 $cm^3 min^{-1}$) at 100 °C for 0.5 h. The NH_3-TPD profile was obtained increasing the temperature from 100 °C to 700 °C at 10 °C min^{-1}. The NH_3 concentration in the effluent was measured by mass spectrometry (MS) in a Baltzers Omnistar unit.

Basic site densities were determined by temperature-programmed desorption of CO_2 (CO_2-TPD). Samples (50 mg) were loaded in a fixed-bed quartz reactor and then pretreated by heating from 25 °C to 300 °C in N_2 flow (60 $cm^3 min^{-1}$) at 10 °C min^{-1}. The final temperature was kept for 1 h. Afterwards, the system was cooled down to room temperature and the samples expose to a CO_2(2%)/N_2 gas stream (60 $cm^3 min^{-1}$) until CO_2 surface saturation. The CO_2-TPD profiles were obtained heating from 25 °C to 800 °C in N_2 (60 $cm^3 min^{-1}$) flow at 10 °C min^{-1}. The effluent gas was analyzed by an on-line Gas Chromatograph SRI 310C with flame ionization detector (FID). Previously to the FID, the outlet gas was converted to methane at 400 °C in a methanation reactor loaded with Ni/Kieselguhr catalyst while passing hydrogen flow.

After SMR experiments, catalysts were characterized by transmission electron microscopy (TEM) and temperature-programmed oxidation (TPO). The TPO profiles were obtained in a fixed-bed quartz reactor loading 50 mg of used catalyst. A continuous flow of O_2(2%)/N_2 (60$cm^3 min^{-1}$) was passed over the sample and the temperature was increased from 25 °C to 800 °C at 10 °C min^{-1}. The outlet gas was converted to CH_4 as it was described above. The measurements by TEM were performed using a FEI Teonai T20 equipment operated at 200 kV.

2.3. Catalytic tests

Catalytic tests were performed in a fixed bed continuous flow reactor operated at atmospheric pressure. A Ni-based catalyst (100–200 mg) was placed in a fixed-bed quartz reactor (i.d.: 6 mm). Catalyst activation was carried out in situ by reduction with H_2 (30 $cm^3 min^{-1}$) at 500 °C or 600 °C for 1 h. After the reduction, a stream of $H_2O/CH_4 = 2$ diluted with H_2 (30 $cm^3 min^{-1}$) was fed to the reactor. The catalytic tests were performed at 500 °C and 600 °C for 2 h. The water at the reactor outlet was trapped using an ice bath. Then, the effluent gas was analyzed using an on-line gas chromatograph GC-8A equipped with a flame ionization detector (FID) and two packed columns (Porapak Q and Porapak QS). The reaction products, CO and CO_2, were separated in the packed column and then converted to CH_4 in a methanation reactor at 400 °C previous to the detection in the FID. The selectivity to CO was defined as $S_{CO} = Y_{CO} \cdot (Y_{CO} + Y_{CO2})^{-1}$, where Y_{CO} and Y_{CO2} are yields in CO and CO_2, respectively. In turn, Y_i is defined as mol of i yielded by CH_4 mol fed. The initial methane conversion rates (r^0, CH_4 mol g_{Ni}^{-1} h^{-1}) were calculated by polynomial regression of the experimental data and subsequent differentiation at time equal to zero. Turn-over frequencies (TOF) were estimated from r^0, atomic weight of nickel (M_{Ni}) and metal dispersion (D) by applying the formula: $TOF = r^0 \cdot M_{Ni}/D$. The catalysts used in SMR experiments are identified by an abbreviation followed by the reduction temperature. For example, NS-500 means Ni/SiO_2 catalyst reduced at 500 °C.

3. Results and discussion

3.1. Sample characterization

The experimental nickel load determined by AA was between 7 and 9 wt% in all of the samples used in this work (Table 1). After impregnation and calcination at 500 °C, the final specific surface areas of samples NS and NA were similar to those of the corresponding supports (Table 1). The specific surface area (*Sg*) of NS was about 20 times higher than that one of NA. Besides, after coprecipitation and thermal decomposition, NMA and NZA mixed oxides have similar *Sg* to the one of NS (Table 1).

The XRD patterns of oxide precursors are shown in Fig. 1. Only a single polycrystalline phase of NiO (JCPDS 22-1189) was formed in the case of NS sample after calcination. In addition, the amorphous halo of SiO_2, due to the scattering of the Si–O–Si structure, was observed at $2\theta < 30°$. In the case of NA sample, two well defined polycrystalline phases were observed: one characteristic of the low surface α-Al_2O_3 (JCPDS 46-1212) and another one corresponding to NiO (JCPDS 22-1189). Instead, broad diffraction lines were observed for the NMA mixed oxide in the range $2\theta = 30–70°$. These lines could be assigned to small NiO crystallites. However, similar XRD patterns were obtained for $MgAl_2O_4$ spinels synthesized at temperatures lower or equal to 600 °C [33]. The X-ray diffractograms for these mixed oxides showed that the diffraction line of highest intensity corresponds to the (400) plane family ($2\theta = 44°$), instead of the (311) plane family ($2\theta = 39°$), which is similar to the X-ray diffactogram obtained for NMA sample in this

Table 1
Physicochemical characterization of nickel samples used in this work.

Sample	*Sg*[a] ($m^2 g^{-1}$)	Ni load (wt%)	*Tr*[b] (°C)	HC_i (cm^3 NPT g^{-1})	*D*[c] (%)	*dp*[d] (nm)
NS	245	8.4	500	0.18	1.1	11–13
NA	12	8	500	0.13	0.8	19
NMA	224	7	500	0.21	1.6	–
			600	0.73	5.5	3–4
NZA	210	8.6	500	0.43	2.6	
			600	0.42	2.6	4–6

[a] Samples calcined at 500 °C.
[b] Reduction temperature.
[c] Metal fraction exposed respect to total Ni estimated by H_2 chemisorption (H/Ni = 1).
[d] Mean particle sizes estimated from TEM histograms.

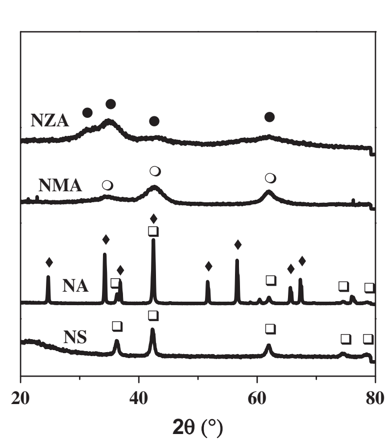

Fig. 1. XRD of samples calcined at 500 °C. (●) Zinc aluminate-like; (○) magnesium aluminate-like; (□) NiO; and (♦) α-Al_2O_3.

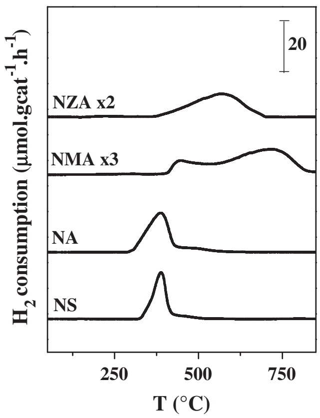

Fig. 2. TPR profiles of samples calcined at 500 °C.

work (Fig. 1). Then, it is very probably that the NMA mixed oxide consists of Ni^{2+} ions and/or very small NiO particles (size less than 4 nm) highly dispersed in a non-stoichiometric Mg–Al spinel matrix. In the case of NZA sample, broad diffraction lines were also obtained between 2θ = 30° and 70°. These peaks fitted very well with the XRD pattern of $ZnAl_2O_4$ with spinel structure (JCPDS 5-669). Similar X-ray diffractogram was obtained in previous works for $ZnAl_2O_4$ prepared by the coprecipitation method and subsequent calcination at 600 °C [30,34]. Then, similar to the case of NMA sample, the most likely is that Ni^{2+} ions are very highly dispersed in the polycrystalline zinc aluminate matrix with spinel-like structure.

TPR profiles are shown in Fig. 2. Both NS and NA samples showed a single peak of H_2 consumption with a maximum around 390–400 °C that is normally assigned to reduction of supported NiO into metal Ni. The broad and asymmetric reduction peaks are probably due to reduction of NiO particles in a wide range of sizes having very low or none interaction with the support [35,36]. Instead, NMA and NZA gave very broad H_2 consumption bands starting at $T \geqslant 400$ °C. The maximum H_2 consumption was reached at 575 °C for NZA and 715 °C for NMA. These TPR results are indicating that: (1) Ni^{2+} ions are strongly interacting with Mg–Al and Zn–Al spinel-like phases in NMA and NZA, respectively; and (2) Ni^{2+} ions are interacting more strongly with the Mg–Al spinel-like phase than with the Zn–Al one. Then, conclusions from TPR profiles are in good agreement with those proposed from XRD results.

The irreversible chemisorbed hydrogen (HC_i) for all of the samples was measured after reduction at 500 °C and 600 °C. The lowest HC_i values were determined for NS, NA and NMA reduced at 500 °C (Table 1). When sample NMA was reduced at 600 °C, the HC_i increased more than three times. According to TPR profiles, it is probably that an important fraction of Ni^{2+} ions remained unreduced in NMA after activation at 500 °C in H_2 flow. When the final reduction temperature was raised to 600 °C, the nickel metallic fraction in NMA dramatically increased and therefore the sample capability for irreversible hydrogen chemisorption also increased. Instead, no difference for hydrogen chemisorption capability was observed with NZA sample reduced at 500 °C and 600 °C. This last result is indicating that: (1) it is likely that almost the major fraction of Ni^{2+} ions are reduced in the NZA sample even at 500 °C; and (2) no sintering takes place when reduction temperature was raised from 500 °C to 600 °C, probably due to the interaction between Ni^0 particles and Zn–Al spinel-like matrix. From the HC_i values, assuming cubic particles and a stoichiometry H/Ni = 1, the metal dispersion was calculated for each sample. Very low dispersions and large mean sizes of metal particles were estimated for samples NS and NA. These values are in good agreement with the large particle sizes observed from TEM histograms (Table 1). These mean particle sizes were even larger for NA sample than for NS one. The metallic dispersions for NMA and NZA were about 3 times higher or more than for NA and NS samples. In the case of NMA and NZA, the dispersion values obtained from H_2 chemisorption cannot be used to estimate a mean particle size, since metal nickel particle are both on surface and in bulk of these samples. Therefore, only TEM measurements were used to estimate the mean metal particle size in NMA and NZA. It was found that only very small particles, with sizes smaller or equal to 6 nm, are present on the sample surfaces prepared by the coprecipitation method (Table 1).

The surface basicity and acidity of all the samples were measured by CO_2-TPD and NH_3-TPD, respectively, and results are summarized in Table 2. The following pattern was found for the surface density of basic sites: NMA > NZA ≅ NA ≫ NS. Instead, the strength of basic sites showed the pattern: NA ≅ NMA > NS ≅ NZA. Besides, only NMA sample showed a detectable density of surface acid sites that desorbed NH_3 with maximum rate at 410 °C.

In summary, NA and NS oxide precursors are constituted by large NiO particles having low interaction with support that are easily reduced at 400 °C or lower temperatures. As a consequence, the reduction in H_2 flow led to a metal phase constituted by large metal nickel particles with low or none interaction with the corresponding support. Instead, in NMA and NZA oxide precursors, Ni^{2+} ions are highly dispersed in a non-stoichiometric spinel-like matrix and they are reduced only at temperatures higher than 500 °C. The reduction in H_2 flow gave as result a very well dispersed metal nickel phase resistant to sintering under H_2 flow at $T \leqslant 600$ °C. All of the samples have surface basic sites of different relative strength and only NMA sample showed a significant acidity. In particular, the weakest basic sites were detected on NZA and NS samples.

Table 2
Basicity and acidity of nickel-based samples by temperature programmed desorption (TPD) of CO_2 and NH_3.

Sample	CO_2-TPD		NH_3-TPD	
	T_M[a] (°C)	$n_b \times 10^4$ (mmol m^{-2})	T_M[a] (°C)	$n_a \times 10^3$ (mmol m^{-2})
NS	140	3.9	–	n.d.
NA	450	57.0	–	n.d.
NMA	400	180.5	410	1.9
NZA	130	52.2	–	n.d.

[a] Temperature at the maximum desorption rate.

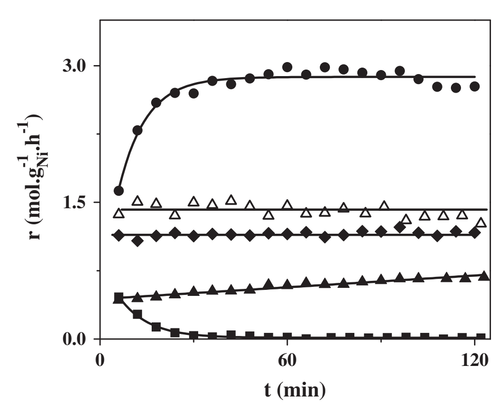

Fig. 3. CH_4 conversion rate in the steam reforming at 500 °C (P = 1 bar, W_{cat} = 100 mg, F_{H2} = 30 cm^3 min^{-1}, H_2O/CH_4 = 2). (■) NS-500, (♦) NA-500, (▲) NMA-500, (△) NMA-600, and (●) NZA-500.

Table 3
Catalytic performance of nickel-based catalysts in steam-methane reforming at 500 °C and 600 °C (P = 1 bar, W_{cat} = 0.1 g; F_{H2} = 30 cm^3 min^{-1}; and H_2O/CH_4 = 2).

Catalysts	T (°C)	r^{0a} (mol g_{Ni}^{-1} h^{-1})	r^{fb} (mol g_{Ni}^{-1} h^{-1})	TOF × 10^{-3} (h^{-1})	S^{0}_{CO} [c]	S_{CO} [d]	C^{e} (%)
NS-500	500	0.86	0.02	4.6	0.98	0.30	0.5
NA-500		1.15	1.10	8.5	0.99	0.16	0.1
NZA-500		0.31	2.88	0.7	0.81	0.20	1.5
NMA-500		0.45	0.69	1.7	0.34	0.10	3.2
NMA-600		1.42	1.42	1.5	0.57	0.20	2.9
NS-600	600	1.41	0.03	7.5	0.89	0.60	29.2
NA-600		1.87	1.87	14.0	0.86	0.35	30.1
NMA-600		7.96	7.96	8.5	0.76	0.50	20.3
NZA-600		7.57	7.57	17.0	0.98	0.50	1.5

[a] Initial methane conversion rate obtained by extrapolation at t = 0.
[b] Steady-state methane conversion rate.
[c] Initial selectivity to CO.
[d] Steady-state selectivity to CO.
[e] Carbon content on used catalysts.

3.2. Catalytic tests

The initial rates for methane conversion at 500 °C followed the pattern: NMA-600 > NA-500 > NS-500 > NMA-500 > NZA-500 (Fig. 3 and Table 3). However, the pattern at the end of the run was: NZA-500 > NMA-600 > NA-500 > NMA-500 ≫ NS-500. The reasons for these changes in the activity pattern can be summarized as follows: (1) catalytic activity of NMA-500, NMA-600 and NA-500 varied very little or remained constant along the 2 h run; (2) methane conversion rate with NS-500 diminished up to almost zero in 30 min; and (3) methane conversion rate with NZA-500 raised by about one order in just 20 min. The very fast deactivation of NS-500 could be due to the following facts: (1) very fast covering of the metal nickel surface by carbonaceous deposits produced by CO disproportionation; and (2) rapid surface oxidation of metal nickel particles by H_2O [9]. The last is the most likely explanation when low coke amounts are produced during SMR. The slight activity increase observed with NMA-500 could be due to incomplete reduction of Ni^{2+} ions strongly interacting with Mg–Al spinel-like, during activation in H_2 flow at 500 °C for 1 h. This assumption is in agreement with TPR profile obtained for the NMA oxide precursor (Fig. 2). In agreement with this assumption, the reaction rate at 500 °C with NMA-600 was about three times higher than with NMA-500 and it kept almost constant during the whole catalytic test (Fig. 3 and Table 3). Similar activity and stability was observed for NMA-600 and NA-500 catalyst. On the contrary, NZA activity increased with time. Analysis by AA showed that about 25% of total Zn was lost after reduction and SMR at 500 °C, probably by sublimation. Then, it is likely that some of the Zn in excess, respect to Zn/Al stoichiometric ratio in $ZnAl_2O_4$, was decorating the metal nickel particles of the NZA-500 catalyst at the beginning of the reaction [37]. In other words, some Zn remained partially covering the metal active surface after reduction in H_2 flow at 500 °C. As the zinc that was covering metal nickel particles was sublimated under reaction conditions at 500 °C, the active surface increased with time and, as a consequence, the methane conversion rate increased, as well.

NA-500 showed the highest TOF of this catalyst series at initial conditions (Table 3). The lowest TOF values were determined for the samples prepared by the coprecipitation method, i.e. NMA-500, NZA-500 and NMA-600. Besides, the CO selectivity (S_{CO}) varied between 0.10 and 0.30, probably due to different activity of each catalyst on CO_2 production reactions, i.e. WGS and CO disproportionation [Eqs. (2) and (3)]. These results are indicating that surface structure is different for each catalyst and the preparation method have an important influence on the type of metal nickel surface exposed and, as a consequence, on the metal site activity. Besides, in all of the cases, S_{CO} diminished with time indicating that metal nickel surface is changing under SMR conditions in such a way that reactions producing CO_2 are favored.

The influence of reaction temperature on the catalytic performance of each nickel-based catalyst was tested by carrying out SMR at 600 °C. In this case, the pattern obtained for methane conversion rate was: NZA-600 = NMA-600 > NA-600 > NS-600 (Fig. 4 and Table 3). It was found that NS-600 suffered a rapid deactivation, even some faster than that observed for NS-500 (Figs. 3 and 4). If reactions (3) and/or (4) are taking place, then this is in agreement with an important increase in the ratio between C(s) production rate and C(s) diffusion rate through metal nickel particles [38,39]. On the contrary, the methane conversion rate with NA-600, NMA-600 and NZA-600 kept practically constant during the whole 2 h-run. It is worth noting that the increase in activity with time observed for NZA-500 (Fig. 3) was not observed with NZA-600 (Fig. 4). This is suggesting that all the zinc in excess, respect to the one forming part of zinc aluminate-like phase, was lost during activation at 600 °C and no zinc decorating the metal nickel particles remained after this treatment. In agreement with this assumption, elemental analysis by AA showed that: (1) about 30% of the total zinc was lost in activation at 600 °C under H_2 flow; and (2) zinc concentration in the used NZA-600 sample after SMR at 600 °C was similar to that one in the sample obtained after activation in H_2 flow at 600 °C. This result is also confirming that, after thermal treatment at 600 °C, the zinc forming part of the zinc aluminate-like phase is stable under reaction conditions.

The TOF at initial conditions for NS-600 and NA-600 was about the same order to that observed for NS-500 and NA-500 (Table 3).

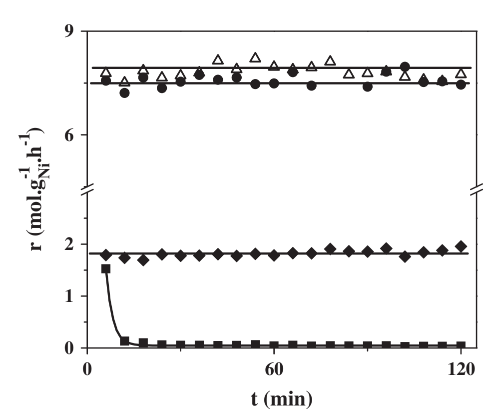

Fig. 4. CH_4 conversion rate in the steam reforming at 600 °C (P = 1 bar, W_{cat} = 100 mg, F_{H2} = 30 cm^3 min^{-1}, H_2O/CH_4 = 2). (■) NS-600, (♦) NA-600, (△) NMA-600, and (●) NZA-600.

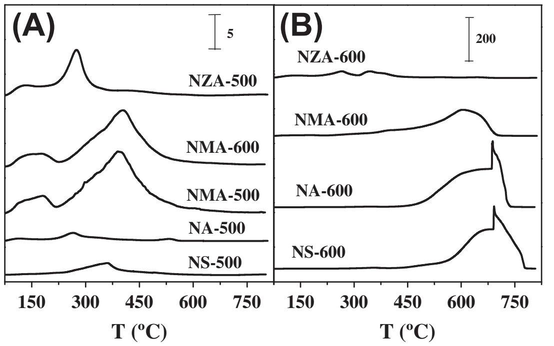

Fig. 5. TPO profiles of the catalysts used in the low temperature steam reforming of CH_4. (A) T = 500 °C and (B) T = 600 °C.

However, an important increment of at least one order was observed in the case of NMA-600 and NZA-600 respect to NMA-500 and NZA-500. This is indicating a strong influence of activation conditions on the intrinsic activity of metal nickel sites in samples prepared by coprecipitation. Again, the lowest selectivity to CO was obtained with NA-600 indicating that this catalyst is the most active of this series for CO_2 production reactions at steady state. Instead, NZA-600 and NMA-600, together with NS-600 showed the highest selectivity to CO at steady state. However, similarly to that observed in SMR at 500 °C, the selectivity to CO diminished with time in all of the cases. This is indicating that a metal surface being more active for CO_2 production was obtained under reaction conditions.

All the above results are indicating that the catalytic performance of metal nickel is showing a complex dependence with the preparation method, metal particle size, support nature, metal–support interaction and activation conditions. Large particles of metal nickel supported on α-Al_2O_3 resulted in one active and stable phase for SMR at low temperatures with low selectivity to CO. Instead, the large particles of metal nickel supported on high surface SiO_2 were non-stable for this reaction under similar conditions. Amazingly, very small nickel particles highly dispersed in a spinel-like phase, as in the case of NMA and NZA catalysts, showed an activity and stability superior to that one of NA, particularly after activation at 600 °C. The last can be explained assuming that the reduction of Ni^{2+} ions, strongly interacting with a spinel-like phase, led to formation of a highly dispersed and stable metallic phase that is very active and selective for SMR at low temperatures. In general, the activity and selectivity to CO of NMA and NZA catalysts is strongly depending on the reduction and reaction conditions. The last is probably due to the important metal–support interaction that is occurring in these samples obtained by coprecipitation method. Furthermore, the methane conversion rate with NZA and NMA was between three and five times higher at 600 °C than at 500 °C, while the TOF increase about one order. The increase in the methane conversion rate was much more important with NZA and NMA than in the case of catalysts constituted by large metal particles. In addition, the selectivity to CO increased two and a half times when the reaction temperature increased. These results indicate that activation energy for SMR on NZA and NMA could be higher than on NA and NS. On the other hand, selectivity to CO is depending on the occurrence of CO disproportionation and WGS reactions, since these are the two

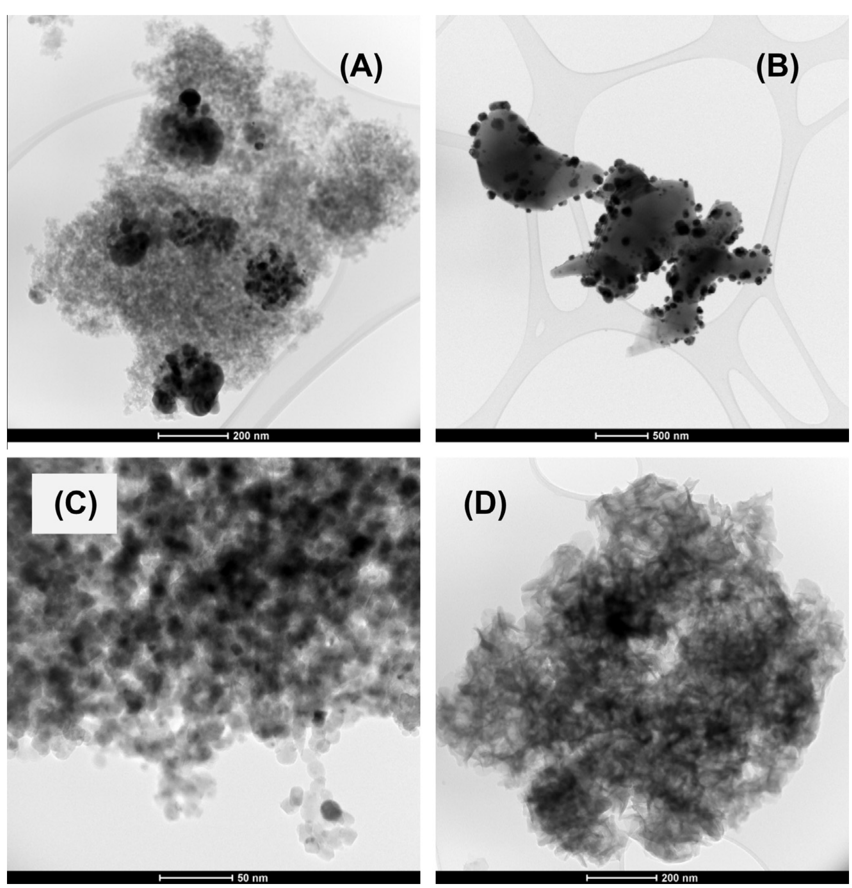

Fig. 6. TEM micrographs of catalysts used in the low temperature steam reforming of CH_4 at 500 °C (A) NS-500; (B) NA-500; (C) NZA-500; and (D) NMA-600.

reactions in which CO is converted into CO_2. Besides, CO selectivity diminished with time in all of the cases, which indicates that not only catalyst activity but also selectivity to CO can be affected by changes in the metal surface during reaction. One reason for these changes is formation of carbon deposits on the catalyst surface. Then, the used samples were analyzed by TPO and TEM in order to determine the amount and type of carbonaceous deposits on each catalyst. The results from TPO and TEM are presented and discussed in the following part.

3.3. Characterization of carbon deposits

The results obtained by TPO are summarized in Table 3 and the corresponding profiles are shown in Fig. 5. The total O_2 consumption was approximated by numerical integration of the TPO profiles. From these values, the pattern obtained for the amount of carbonaceous deposits on the catalysts used in SMR at 500 °C was the following: NMA-500 ≅ NMA-600 > NZA-500 > NS-500 ≅ NA-500 (Fig. 5A, Table 3). In all of the cases, the coke formed during SMR at 500 °C was lower than 3.2% and it was burn-out at temperatures below 500 °C. In particular, the coke deposited on NZA-500 and NA-500 was mainly removed between 200 °C and 300 °C. The O_2 consumption peak for the used NS-500, NMA-500 and NMA-600 samples showed a maximum at around 370–400 °C (Fig. 5A). These results are indicating that the coke formed in reaction at 500 °C was amorphous and mainly deposited on the supports [40,41]. This was confirmed by TEM since the typical nanofibers formed on nickel-based catalysts under SMR conditions were not observed on the surface of the used catalysts (Fig. 6). In the case of samples NS-500 and NA-500, only large metal nickel particles in the range of 10–30 nm were observed and practically no evidence of carbon deposits was found in agreement with the low content determined by TPO (Fig. 6, micrographs A and B). In the case of NZA-500, NMA-500 and NMA-600, the metal nickel particles are still between 3 and 6 nm and only coke of amorphous nature could be observed, in agreement with TPO results (Fig. 6, micrographs C and D). In summary, the following facts were observed after SMR at 500 °C: (1) the highest amount of coke was around 3% and it was formed over the NMA catalysts, which showed both surface acidity and basicity; and (2) the coke has always amorphous nature and no carbon nanofibers were formed under these conditions. It is worth noting that not only the amount but the burn temperature of coke on NMA-500 and NMA-600 are very similar, indicating that the coke formed on these two samples has similar nature. NH_3-TPD and CO_2-TPD experiments showed that surface acidity of medium strength was observed only on NMA samples (Table 2). This can explain the highest formation of amorphous coke on the oxide matrix of NMA-500 and NMA-600 in SMR at 500 °C, which is in agreement with previous works [19]. In line with this, the low amount of amorphous coke over NZA-500, NA-500 and NS-500 could be due to both the absence of acidity and low basicity on the surface of these catalysts.

When SMR was carried out at 600 °C, the patterns for the burning temperature and total O_2 consumption were completely different to that one observed after SMR at 500 °C: NS-600 ≅ NA-600 > NMA-600 ≫ NZA-600 (Fig. 5B, Table 3). For NZA, all the coke was burned below 400 °C, which is indicative that only amorphous carbon was formed on this catalyst. Instead, the O_2 consumption with NMA-600 was observed between 500 °C and 700 °C. In the case of NS and NA, most of the deposited carbon was burned

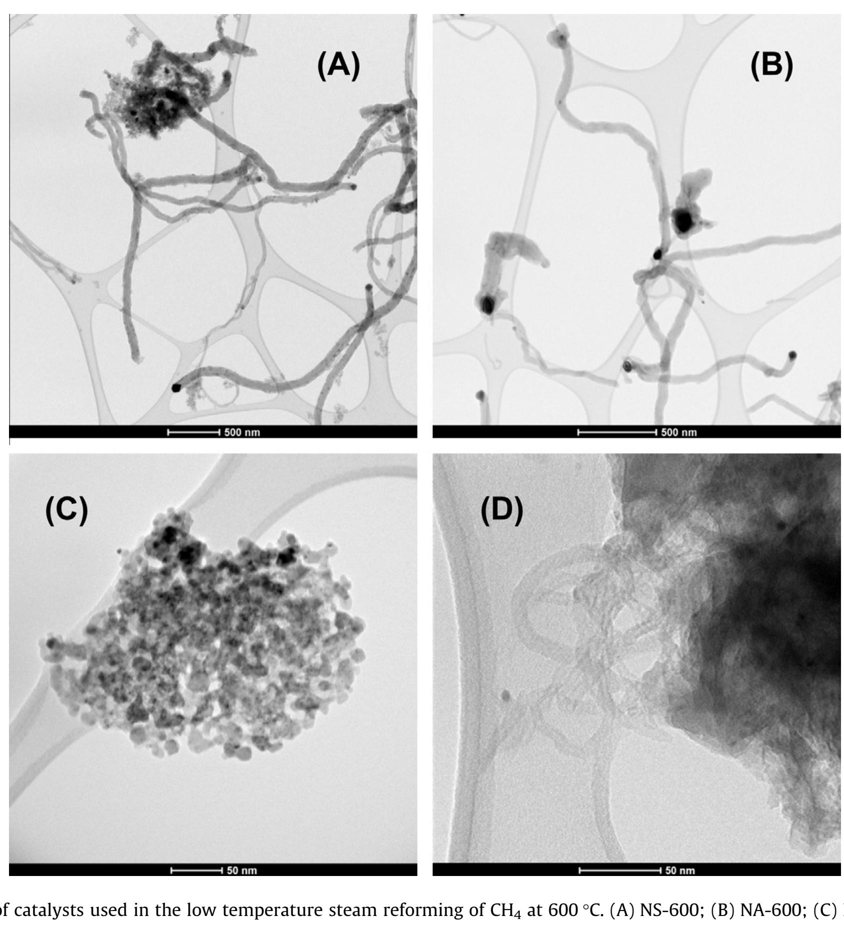

Fig. 7. TEM micrographs of catalysts used in the low temperature steam reforming of CH_4 at 600 °C. (A) NS-600; (B) NA-600; (C) NZA-600; and (D) NMA-600.

between 600 °C and 750 °C. In previous works, these bands have been normally assigned to oxidation of carbon nanotubes and nanofibers [40,41].

The TEM micrographs showed that the size intervals for the metal nickel particles, in samples activated and used at 600 °C, are in the same range as the samples activated and used at 500 °C (Figs. 6 and 7). Thus, the metal particle in NS-600 and NA-600 are in the range of 10–30 nm, while the metal particle in NMA and NZA remained between 4 and 5 nm. These results are indicating that no important sintering of metal nickel particles was observed due to temperature increase from 500 to 600 °C. However, nanofibers with a diameter similar to the corresponding metal particle sizes were clearly observed in samples NA-600, NS-600 and NMA-600 (Fig. 7, micrographs A, B and D). Amazingly, no nanofibers but only amorphous coke in small amounts was observed on NZA-600 (Fig. 7, micrograph C), with similar nature to that one formed on NZA-500. The low amount of carbon deposits detected over used NMA-600 and NZA-600 catalysts, respect to NA-600 and NS-600, can be due to: (1) the particle size and the high metal–spinel interaction are inhibiting C(s) dissolution and diffusion and, as a consequence, formation of nanofibers [42–44]; (2) the rate of C(s) gasification at 600 °C on the metal nickel surface of NZA and NMA is higher than that one on NA and NS catalysts [45]; and (3) the CO disproportionation and CH_4 decomposition are inhibited on NZA and NMA. In any case, these facts or at least some of them seem to be much more important on NZA than on NMA, which is indicative that the type of spinel-like phase and metal–spinel interaction play a very important role on the type and amount of carbon deposited on the catalyst surface. Then, the differences in formation rate and type of carbonaceous deposits can be attributed to the distinct active phases exposed on NZA and NMA catalysts.

In summary, these results showed that the low selectivity to CO at 500 °C is explained by a very important contribution of WGS, reaction (2), since the amount of carbon deposits is very low in general and so the contribution of CO disproportionation, reaction (3), to CO_2 production would not be important under these conditions. Instead, according to the amount of carbonaceous deposits detected, the influence of CO disproportionation on selectivity seems to increase at 600 °C, especially in the case of NA-600 and NS-600 and so it could be the main source for CO_2 production. However, at this temperature, the contribution of CH_4 decomposition on C(s) production cannot be disregarded. The amount of carbon deposited on NMA-600 is lower than on NA-600. It is then possible that the higher selectivity to CO with NMA is due to a lower extent of CO disproportionation respect to NA-600 and due to some gasification of C(s) by interaction with H_2O and/or H_2 [45,46]. Finally, the selectivity to CO with NZA-600 was similar to the one obtained with NMA-600, but very little amorphous coke was observed after SMR at 600 °C. One possibility is that CO disproportionation took place on NZA-600 but carbon gasification was much faster with NZA than with NMA.

4. Conclusions

In this work, several Ni-based catalysts with different metal particle size and metal–support interaction were prepared by impregnation and coprecipitation techniques. Large metal nickel particles with none interaction with SiO_2 led to a very unstable catalyst, which is deactivated very fast by either surface oxidation or carbonaceous deposits. Active and stable catalysts for steam-methane reforming between 500 and 600 °C were obtained when very small metal nickel particles are in intimate contact with a zinc aluminate-like or magnesium aluminate-like matrix. In addition, these catalysts give the lowest production of carbonaceous deposits. In summary, carbon production is reduced when the active phase is basically composed of very small metal nickel particles obtained by reduction of Ni^{2+} ions strongly interacting with the spinel-like matrix. In particular, Ni–Zn–Al catalyst showed the highest activity of the series with the lowest production of carbonaceous deposits in the range 500–600 °C. This catalyst must be activated at 600 °C, previous to reaction, in order to prevent zinc sublimation during steam reforming. In addition, sintering is not occurring in this catalyst under reaction conditions since the metal–support interaction is the proper to avoid particle migration and subsequent coalescence. Then, Ni–Zn–Al activated by reduction at 600 °C becomes a suitable catalyst for use in the low temperature zone of a methane reformer or in a pre-reformer unit. The use of a catalyst with this catalytic performance could reduce the problems usually appearing in the start-up of industrial reformers.

Acknowledgements

We thank to Universidad Nacional del Litoral (UNL), Consejo Nacional de Investigaciones Científicas y Técnicas (CONICET) and Agencia Nacional de Promoción Científica y Tecnológica (ANPCyT), Argentina, for the financial support to this work.

References

[1] C.H. Bartholomew, R.J. Farrauto, in: Fundamentals of Industrial Catalytic Processes, John Willey and Sons, Hoboken, New Jersey, USA, 2006 (Chapter 6).
[2] www1.eere.energy.gov/hydrogenandfuelcells/production/printable_versions/natural_gas.html, November 20, 2012.
[3] Ullmann's Encyclopedia of Industrial Chemistry, seventh ed., Wiley-VCH, 2013.
[4] J.R. Rostrup-Nielsen, in: J.R. Anderson, M. Boudart (Eds.), Catalysis, Science and Technology, vol. 5, Springer, Berlín, 1984 (Chapter 1).
[5] J.R. Rostrup-Nielsen, J. Sehested, Wisker carbon revisited, Stud. Surf. Sci. Catal. 139 (2001) 1–12.
[6] J.R. Rostrup-Nielsen, Th.S. Christensen, Ib. Dybkjaer, Steam reforming of liquid hydrocarbons, Stud. Surf. Sci. Catal. 113 (1998) 81–95.
[7] K.O. Christensen, D. Chen, R. Lødeng, A. Holmen, Effect of supports and Ni crystal size on carbon formation and sintering during steam methane reforming, Appl. Catal. A: Gen. 314 (2006) 9–22.
[8] H.-W. Kim, K.-M. Kang, H.-Y. Kwak, J.H. Kim, Preparation of supported Ni catalysts on various metal oxides with core/shell structures and their tests for the steam reforming of methane, Chem. Eng. J. 168 (2011) 775–783.
[9] Y. Matsumura, T. Nakamori, Steam reforming of methane over nickel catalysts at low reaction temperature, Appl. Catal. A: Gen. 258 (2004) 107–114.
[10] H.-S. Roh, K.-W. Jun, W.-S. Dong, S.-E. Park, Y.-S. Baek, Highly stable Ni catalyst supported on Ce–ZrO_2 for oxy-steam reforming of methane, Catal. Lett. 74 (1–2) (2001) 31–36.
[11] N. Laosiripojana, S. Assabumrungrat, Catalytic steam reforming of methane, methanol, and ethanol over Ni/YSZ: the possible use of these fuels in internal reforming SOFC, J. Power Sources 163 (2007) 943–951.
[12] A. Al-Ubaid, E.E. Wolf, Steam reforming of methane on reduced non-stoichiometric nickel aluminate catalysts, Appl. Catal. 40 (1988) 73–85.
[13] K. Hou, R. Hughes, The kinetics of methane steam reforming over a Ni/α-Al_2O_3 catalyst, Chem. Eng. J. 82 (2001) 311–328.
[14] K. Lertwittayanon, D. Atong, P. Aungkavattana, T. Wasanapiarnpong, S. Wadaa, V. Sricharoenchaikul, Effect of CaO–ZrO_2 addition to Ni supported on γ-Al_2O_3 by sequential impregnation in steam methane reforming, Int. J. Hydrogen Energy 35 (2010) 12277–12285.
[15] J. Comas, M.L. Dieuzeide, G. Baronetti, M. Laborde, N. Amadeo, Methane steam reforming and ethanol steam reforming using a Ni(II)–Al(III) catalyst prepared from lamellar double hydroxides, Chem. Eng. J. 118 (2006) 11–15.
[16] X. Guo, Y. Sun, Y. Yu, X. Zhu, C. Liu, Carbon formation and steam reforming of methane on silica supported nickel catalysts, Catal. Commun. 19 (2012) 61–65.
[17] A. Fonseca, E.M. Assaf, Production of the hydrogen by methane steam reforming over nickel catalysts prepared from hydrotalcite precursors, J. Power Sources 142 (2005) 154–159.
[18] S.S. Maluf, E.M. Assaf, Ni catalysts with Mo promoter for methane steam reforming, Fuel 88 (2009) 1547–1553.
[19] J.A. Lercher, J.H. Bitter, W. Hally, W. Niessen, K. Seshan, Design of stable catalysts for methane–carbon dioxide reforming, Stud. Surf. Sci. Catal. 101 (1996) 463–472.
[20] J.R. Rostrup-Nielsen, J. Sehested, J.K. Nørskov, Hydrogen and synthesis gas by steam- and CO_2 reforming, Adv. Catal. 47 (2002) 65–139.
[21] J. Sehested, J.A.P. Gelten, I.N. Remediakis, H. Bengaard, J.K. Nørskvo, Sintering of nickel steam-reforming catalysts: effects of temperature and steam and hydrogen pressures, J. Catal. 223 (2004) 432–443.

[22] K. Takehira, T. Shishido, P. Wang, T. Kosaka, K. Takaki, Autothermal reforming of CH_4 over supported Ni catalysts prepared from Mg–Al hydrotalcite-like anionic clay, J. Catal. 221 (2004) 43–54.
[23] F. Basile, G. Fornasari, V. Rosetti, F. Trifirò, A. Vaccari, Effect of the Mg/Al ratio of the hydrotalcite-type precursor on the dispersion and activity of Rh and Ru catalysts for the partial oxidation of methane, Catal. Today 91–92 (2004) 293–297.
[24] A.I. Tsyganok, M. Inaba, T. Tsunoda, K. Suzuki, K. Takehira, T. Hayakawa, Combined partial oxidation and dry reforming of methane to synthesis gas over noble metals supported on Mg–Al mixed oxide, Appl. Catal. A: Gen. 275 (2004) 149–155.
[25] L. Roses, F. Gallucci, G. Manzolini, M. van Sint Annaland, Experimental study of steam methane reforming in a Pd-based fluidized bed membrane reactor, Chem. Eng. J. 222 (2013) 307–320.
[26] S. Miura, Y. Umemura, Y. Shiratori, T. Kitaoka, In situ synthesis of Ni/MgO catalysts on inorganic paper-like matrix for methane steam reforming, Chem. Eng. J. 229 (2013) 515–521.
[27] Y.S. Cheng, M.A. Peña, K.L. Yeung, Hydrogen production from partial oxidation of methane in a membrane reactor, J. Taiwan Inst. Chem. Eng. 40 (2009) 281–288.
[28] S.C. Dantas, K.A. Resende, R.L. Rossi, A.J. Assis, C.E. Hori, Hydrogen production from oxidative reforming of methane on supported nickel catalysts: an experimental and modeling study, Chem. Eng. J. 197 (2012) 407–413.
[29] M. Mbodji, J.M. Commenge, L. Falk, D. Di Marco, F. Rossignol, L. Prost, S. Valentín, R. Joly, P. Del-Gallo, Steam methane reforming reaction process intensification by using a milistructured reactor: experimental setup and model validation for global kinetic rate estimation, Chem. Eng. J. 207–208 (2012) 871–884.
[30] J.C. Rodríguez, A.J. Marchi, A. Borgna, A. Monzón, Effect of Zn content on catalytic activity and physicochemical properties of Ni-based catalysts for selective hydrogenation of acetylene, J. Catal. 171 (1997) 268–278.
[31] A.J. Marchi, D.A. Gordo, A.F. Trasarti, C.R. Apesteguía, Liquid phase hydrogenation of cinnamaldehyde on Cu-based catalysts, Appl. Catal. A: Gen. 249 (2003) 53–67.
[32] T.F. Garetto, E. Rincón, C.R. Apesteguía, Deep oxidation of propane on Pt-supported catalysts: drastic turnover rate enhancement using zeolite supports, Appl. Catal. B: Environ. 48 (2004) 167–174.
[33] A. Saberi, F. Golestani-Fard, H. Sarpoolakya, M. Willert-Porada, Th. Gerdes, R. Simonc, Chemical synthesis of nanocrystalline magnesium aluminate spinel via nitrate–citrate combustion route, J. Alloys Compd. 462 (2008) 142–146.
[34] J. Wrzyszcz, M. Zawadzki, J. Trawczyński, H. Grabowska, W. Mišta, Some catalytic properties of hydrothermally synthesised zinc aluminate spinel, Appl. Catal. A: Gen. 210 (2001) 263–269.
[35] K. Hadjiivanov, M. Mihaylov, F. Klissurski, P. Stefanov, N. Abadjieva, E. Vassileva, L. Mintchev, Characterization of Ni/SiO_2 catalysts prepared by successive deposition and reduction of Ni^{2+} ions, J. Catal. 185 (1999) 314–323.
[36] N.M. Bertero, A.F. Trasarti, C.R. Apesteguia, A.J. Marchi, Solvent effect in the liquid-phase hydrogenation of acetophenone over Ni/SiO_2: a comprehensive study of the phenomenon, Appl. Catal. A: Gen. 394 (2011) 228–238.
[37] E.L. Rodrigues, A.J. Marchi, C.R. Apesteguia, J.M.C. Bueno, Promoting effect of zinc on the vapor-phase hydrogenation of crotonaldehyde over copper-based catalysts, Appl. Catal. A: Gen. 294 (2005) 197–207.
[38] K.P. De Jong, J.W. Geus, Carbon nanofibers: catalytic synthesisand applications, Catal. Rev. Sci. Eng. 42 (2000) 481–510.
[39] A. Monzon, G. Lolli, S. Cosma, S.B. Mohamed, D.E. Resasco, Kinetic modeling of the SWNT growth by CO disproportionation on CoMo catalysts, J. Nanosci. Nanotechnol. 8 (2008) 6141–6152.
[40] B. Kitiyanan, W.E. Alvarez, J.H. Harwell, D.E. Resasco, Controlled production of single-wall carbon nanotubes by catalytic decomposition of CO on bimetallic Co–Mo catalysts, Chem. Phys. Lett. 317 (2000) 497–503.
[41] S. Tang, Z. Zhong, Z. Xiong, L. Sun, L. Liu, J. Lin, Z.X. Shen, K.L. Tan, Controlled growth of single-walled carbon nanotubes by catalytic decomposition of CH_4 over Mo/Co/MgO catalysts, Chem. Phys. Lett. 350 (2001) 19–26.
[42] D. Chen, K.O. Christensen, E. Ochoa-Fernández, Z. Yu, B. Tøtdal, N. Latorre, A. Monzon, A. Holmen, Synthesis of carbon nanofibers: effects of Ni crystal size during methane decomposition, J. Catal. 229 (2005) 82–96.
[43] N. Latorre, E. Romeo, F. Cazaña, T. Ubieto, C. Royo, J.I. Villacampa, A. Monzon, Carbon nanotube growth by catalytic chemical vapor deposition: a phenomenological kinetic model, J. Phys. Chem. C 114 (2010) 4773–4782.
[44] J.I. Villacampa, C. Royo, E. Romeo, J.A. Montoya, P. Del Angel, A. Monzón, Catalytic decomposition of methane over $Ni–Al_2O_3$ coprecipitated catalysts: reaction and regeneration studies, Appl. Catal. A: Gen. 252 (2003) 363–383.
[45] J.L. Figueiredo, Gasification of carbon deposits on catalysts and metal surfaces, Fuel 65 (1986) 1377–1382.
[46] G. Domazetis, B.D. James, J. Liesegang, M. Raoarun, M. Kuiper, I.D. Potter, D. Oehme, Experimental studies and molecular modelling of catalytic steam gasification of brown coal containing iron species, Fuel 93 (2012) 404–414.